ISSN 0915-633X

NATIONAL INSTITUTE FOR FUSION SCIENCE

Formation of Positive Radial Electric Field by Electron Cyclotron Heating in Compact Helical System

H. Idei, K. Ida, H. Sanuki, S. Kubo, H. Yamada,
H. Iguchi, S. Morita, S. Okamura, R. Akiyama,
H. Arimoto, K. Matsuoka, K. Nishimura,
K. Ohkubo, C. Takahashi, Y. Takita,
K. Toi, K. Tsumori and I. Yamada

(Received - June 24, 1994)

NIFS-291 July 1994

RESEARCH REPORT
NIFS Series

NAGOYA, JAPAN

Formation of Positive Radial Electric Field by Electron Cyclotron Heating in Compact Helical System

H. Idei, K. Ida, H. Sanuki, S. Kubo, H. Yamada, H. Iguchi, S. Morita, S. Okamura, R. Akiyama, H. Arimoto,[a)] K. Matsuoka, K. Nishimura, K. Ohkubo, C. Takahashi, Y. Takita, K. Toi, K. Tsumori and I. Yamada

National Institute for Fusion Science, Nagoya 464-01, Japan

a)*Plasma Science Center, Nagoya University, Nagoya 464-01, Japan*

Abstract

The radial electric field is driven to positive value by off-axis second harmonic electron cyclotron heating(ECH) in the Compact Helical System [*Plasma Physics and Controlled Nuclear Fusion Research, 1988*, Nice(International Atomic Energy Agency, Vienna, 1989) Vol.II p.411]. The observed positive electric field is associated with the outward particle flux enhanced with ECH. The enhanced particle flux triggered by the production of the electrons accelerated perpendicularly to the magnetic field with ECH results in the change of the electric field.

Keywords: radial electric field, density pump-out, electron cyclotron heating, heliotron/torsatron, particle flux,

I. INTRODUCTION

In stellarator devices, non-ambipolar property of radial fluxes induces intrinsic radial electric field. The neoclassical theory suggests that such electric field reduces the helical ripple loss, and consequently improves the plasma confinement.[1–3] There are generally two stable states in the stellarator plasmas which satisfy ambipolarity equation. They are called the ion root(negative electric field) and the electron root(positive electric field).[3] In a stellarator reactor, it is an important scenario to attain the electron root because the higher energy confinement time is expected with positive electric field.[1] Various observations on the radial electric field have been reported in stellarator devices. In Heliotron-E device,[4] the radial electric field at $r \simeq 0.7\text{-}0.9a$ is found to be positive(the electron root) for the low density plasma($n_e < 1 \times 10^{13}\text{cm}^{-3}$), and negative(the ion root) for the high density plasma($n_e > 2 \times 10^{13}\text{cm}^{-3}$).[5] In Wendelstein VII-A stellarator,[6] the observed electric field in the plasma with electron cyclotron heating(ECH) (at $n_e \sim 5 \times 10^{13}$ cm^{-3}) is consistent with a theoretical prediction.[7] In Advanced Toroidal Facility(ATF),[8] the positive electric field is observed for the low-density plasma with ECH at $n_e \sim 5 \times 10^{12}$ cm^{-3}.[9] In Compact Helical System(CHS),[10] the observed radial electric field is negative in the typical neutral beam(NB) heated plasmas.[11] The electric field becomes more negative near the plasma edge for the higher electron densities.

However, those experimental results have not certified the clear effect of the radial electric field on the confinement. In order to study this effect, it is necessary to have a method which can control the radial electric field externally. More recently, the transition of electric field from the ion to the electron root is found when the particle flux is sufficiently enhanced by superposition of ECH on NB heated plasmas in CHS.[12] The transition of the radial electric field was observed as the ECH power was increased. It suggests that ECH can be a powerful tool for such studies. It is important that the relationship between the particle flux and the electric field and the physical process of particle flux enhancement are clarified. Density pump-out due to ECH has been generally observed in both tokamaks and stellarators.[13–16] In PDX tokamak,[17] the density pump-out was clearly observed at the superposition of ECH on the NB heated plasmas and the ohmically heated ones at the intermediate density(central density between $0.7 \times 10^{13}\mathrm{cm}^{-3}$ to $2 \times 10^{13}\mathrm{cm}^{-3}$).[13] In CHS, it is reported that the density pump-out or the degradation of the particle confinement is triggered by the production of electrons accelerated perpendicularly to the magnetic field with ECH.[16]

In this paper, we present the formation of the positive radial electric field through enhancing the particle flux due to ECH and its relation with resonance positions, power and injection modes. The physical process in the particle flux enhancement due to ECH and the relationship between the particle flux and the electric field are also discussed.

Experimental setup is described in Sec.II and the experimental results are presented in Sec.III. The physical process for the particle flux enhanced with ECH and the resultant electric field are discussed in Sec.IV. In Sec.V, conclusion is described.

II. EXPERIMENTAL SETUP

CHS is a heliotron/torsatron device with a pole number of l=2, a toroidal period number m=8 and an aspect ratio of 5. In this study, the major radius R is 92cm and the averaged minor radius a is 19cm. The second harmonic ECH is carried out with the 53.2GHz gyrotron of the maximum pulse width of 100ms. Here, more than 60 % of the injection power is focused as a Gaussian beam with a desired ordinary(O-) or extraordinary(X-) mode whose waist size is 2.5cm and waist position is at the mid-plane of CHS vacuum vessel. The focusing system is composed of a stair cut Vlasov antenna, an improved reflecting mirror and a steerable focusing mirror.[18] The injections of O- or X-mode become possible by using a plane reflector or a reflecting corrugated polarizer, respectively. The focal points of ECH are controlled using the steerable focusing mirror. The 7.5MHz ion cyclotron range of frequency(ICRF) is used for the pre-ionization of plasmas in this study.[19] The NB is tangentially injected to sustain the plasmas. The line-averaged electron density is measured with an HCN laser interferometer. Electron density and temperature profiles are measured with a single-channel Thomson scattering (TS) system. Poloidal rotation and ion temperature

profiles are measured with a charge exchange spectroscopy (CXS) diagnostic using the heating beam with a time resolution $\Delta t_{\rm CXS} = 16.7$ms.[20] The radial electric field is evaluated from the observed poloidal rotation and the ion pressure gradient using a radial momentum balance equation for a fully ionized carbon. Since a toroidal rotation damps due to a viscosity caused by the helical ripple, its contribution is usually small and negligible in the momentum balance equation.[21]

III. EXPERIMENTAL RESULTS

A. Effect of ECH Resonance Positions

The ripple top of the magnetic field strength along the field line at $r = 0.5a$ is located at high field side near the mid-plane of the torus as shown in Fig.1. Another resonance configuration located at the low field side is also shown in the figure. Although resonance areas in the another configuration do not necessarily correspond to the bottom of the magnetic field strength due to both the toroidal and helical ripples, the resonance is called the ripple bottom resonance in contrast with the ripple top one here. The central toroidal magnetic fields $B_{\rm t}$ are 0.75T and 0.93T for the ripple top and bottom resonances, respectively. The second harmonic ECH are superposed on the NB heated plasmas in order to control the particle flux. The injection power of ECH $P_{\rm ECH}$ is 140kW in this experiment. The densities of the NB heated

target plasmas are adjusted below the cut-off density for the second harmonic X-mode ECH($\sim 9.5 \times 10^{12}\mathrm{cm}^{-3}$). Figure 2 shows the radial profiles of electron density $n_e(\rho)$ at 15ms after the ECH is turned on for the two resonance configurations. Here, ρ is a normalized radius calculated with finite β equilibrium code, VMEC[22,23] As a reference plasma, we choose the NB heated plasma without ECH at B_t=0.93T with the same line-averaged density as that for the plasma with ECH to eliminate the density dependence of the radial electric field. The density decrements are observed in both the configurations, but the decrement in the superposition of ECH for the ripple bottom resonance is larger than that for the ripple top one. Figure 3 shows the radial profiles of electron temperature $T_e(\rho)$, ion temperature $T_i(\rho)$, poloidal rotation velocity $v_\theta(\rho)$ and the electric field $E_r(\rho)$ evaluated by the momentum balance equation. The large positive electric field($\sim$ 44V cm^{-1} at ρ=0.82) is observed in the case of the ripple bottom resonance where the strong particle flux enhancement with ECH is expected.

B. Effect of ECH Power and Injection Mode

The transition of the radial electric field to positive value has been observed as the ECH power has been increased.[12] Figure 4 shows the radial profiles of radial electric field $E_r(\rho)$ at 15ms after the ECH is turned on for the reference plasma and those with P_{ECH} = 85 and 140kW. The line-averaged densities for the target plasmas are kept constant. The large positive electric field is observed for the plasma with P_{ECH}=140kW

while the electric field for the reference plasma and that with P_{ECH}=85kW is about zero or small negative value.

The second harmonic ECH with the X- and O-mode injections at the ripple bottom resonance are superposed on the NB heated plasmas with P_{ECH}=140 and 170kW, respectively. Figure 5(a) shows the time evolutions of the decrement in the line-averaged density $\Delta\bar{n}_e$ for O- and X-mode injections. The corresponding radial profiles of poloidal rotation velocity $v_\theta(\rho)$ at 15ms after the ECH is turned on are shown in Fig.5(b). In X-mode injection where the density decay is large, the plasma clearly rotate in the ion-diamagnetic direction which corresponds to the positive electric field.

IV. DISCUSSIONS

A. Particle Flux Enhanced with ECH

One of the candidates to explain the mechanism of the density pump-out is the outward flux due to the poor confinement of perpendicularly accelerated electrons with ECH.[24] The profile of the enhanced particle flux $\Gamma_{ECH}(\rho)$ is deduced from the equation of continuity using the density decay.[12] The evaluated profiles $\Gamma_{ECH}(\rho)$ are shown in Fig.6 for the plasmas with P_{ECH}=85 and 140kW in the power scan experiment. The neoclassical flux $\Gamma^{NC}(\rho)$ for the target plasma in the figure is estimated using the connection formula of neoclassical transport that covers the whole collisionality regime

[Eqs.(6)-(11) in Ref.2], where the experimental data $n_e(\rho)$, $T_e(\rho)$ and $T_i(\rho)$ are taken into account and a single helicity model is used. It is noted that electrons are in the $1/\nu$ regime for the plasma with ECH at the ripple bottom resonance(the electron collisionality $\nu_{*\,e}[= (qR/\varepsilon_h^{1.5} v_{th})\nu] > 0.5$) at $\rho \simeq$0.6-0.9, while ions are in plateau regime. Here, ν is the pitch angle scattering frequency by the collisions, q is a safety factor, ε_h is the helical ripple and v_{th} is a electron thermal velocity. On the other hand, both ions and electrons for the reference and the target plasma are in plateau regime in the whole plasma region.

In the low-aspect-ratio heliotron/torsatron like CHS, the drift orbits of the helically trapped electrons markedly deviate from the magnetic surfaces.[25] Therefore, the helically trapped electrons and the transition(from passing to helically trapped) electrons produced by ECH to be rare collisional ones are poorly confined. The electron loss predicted theoretically is realized in the rare collision limit.[24] Firstly, we discuss the possibility of creating the rare collisional electrons with ECH. The theory of nonlinear interaction is developed in a parabolic magnetic well.[26] The nonlinear interaction is characterized by a large periodic energy excursions with a period of $2\pi/\nu_{rf}$ and the peak energy ξ_{exc}. The net heating is realized by Coulomb collisions (or other randomization process). It was shown in Ref.26 that the nonlinear interaction is strong and is larger than the quasiliner contribution when the effective randomization fre-

quency $\nu_{\rm eff}(\equiv \nu/\Delta_{\rm r}^2)$ is comparable to the energy excursion frequency $\nu_{\rm rf}$(in the region of $10^{-1} < \nu_{\rm eff}/\nu_{\rm rf} < 10^3$) for the second harmonic ECH near the bottom resonance of the magnetic well. Here, $\Delta_{\rm r}$ is the width of the resonance in pitch-angle space. As a special case, the effect of the nonlinear interaction at the the ripple bottom resonance tuned very well can be evaluated on the basis of the test particle model under the following assumptions.:

- The magnetic well is assumed to be the parabolic one near the ripple bottom (well length $L \sim [(1-\varepsilon_{\rm t}-\varepsilon_{\rm h})R^2/\varepsilon_{\rm h}m^2]^{0.5}$, where $\varepsilon_{\rm t}$ is the toroidal ripple.).

- The electric field of the wave is uniform with that of the beam center at the waist point E_0 which is estimated from the ECH power $P_{\rm focus}(\sim 60\%$ of the injection power $P_{\rm ECH})$ focused as the Gaussian beam with waist size $\omega_0 = 2.5$cm using the following relation,

$$P_{\rm focus} \sim \frac{\pi\omega_0^2}{2Z_0}E_0^2, \tag{1}$$

where Z_0 is a wave impedance. (Here, we use $P_{\rm focus}$=60kW.)

- The temperature and density are 300eV and $1 \times 10^{13}{\rm cm}^{-3}$ for the background plasma, respectively. The similar parameters are obtained for the target plasmas.

• The test electron is deeply trapped in the magnetic bottom satisfying the resonant condition ($|v_{//}/v_{\perp}| < \Delta_r/2$, where $v_{//}$ and $v_{\perp}$ are the parallel and perpendicular velocities, respectively). For instance, Δ_r is evaluated to be 0.12 for the initial perpendicular energy of the test electron $E_{\perp}$ =300eV.

The increase in the perpendicular energy $< \Delta E_{\perp} >$ for the test electron is derived as follows.

$$< \Delta E_{\perp} >= \frac{\xi_{exc}}{2}[1 - \exp(-\beta)\cos\beta], \tag{2}$$

where β is $(\nu_{eff}/\nu_{rf})^{-0.5}$. A Lorentz collision model is taken as the Coulomb collision process which realizes the net heating. The ratio ν_{eff}/ν_{rf} and the energy increase $< \Delta E_{\perp} >$ by the nonlinear interaction are shown in Fig.7 as a function of the initial energy $E_{\perp}$ of the test electron. Under the process mentioned above, ν_{eff} can become comparable to ν_{rf}, and the test electrons with $E_{\perp}$=300eV(at $\nu_{*e} \sim 2$) is accelerated up to about 780eV(at $\nu_{*e} \sim 0.4$). As shown in Fig.7, since the excursion time $\tau_{rf}(\equiv 1/\nu_{rf})$ is little less than the passing time τ_{pas} of the electrons through the resonance area(in the beam waist), the nonlinear interaction may affect not only the helically trapped electron in the magnetic well but also the passing electrons. However, the above assumptions that are necessary for the evaluation are not always valid for the interaction at the resonances in the ripple bottom configuration. Also, we have to treat the Fokker-Planck equation in order to discuss quantitatively the particle flux enhanced with ECH. Since

the deviation of the drift orbits from the magnetic surface due to which the particle flux enhancement is predicted in the rare collision limit is large in the low-aspect-ratio device like CHS, the particle distribution in the Fokker-Planck equation can not be treated as the function of the only radial position.

The observed density decrease in the ripple bottom case is larger than that in the ripple top one. The density decay with O-mode ECH is observed to be weak. Next, the effects of the resonant magnetic configuration and injection modes of ECH on the particle flux enhancement with ECH are discussed. The helically trapped electrons are more easily created with ECH at the ripple bottom resonance than at the ripple top one, even though the only effect of the magnetic configuration is taken into consideration. At the ripple top resonance, the passing electrons can not transit into the helically trapped and transition ones with increase of the perpendicular energy by ECH. If the helically trapped electrons are created near the mid-plane, the ECH generates the outward(inward) particle flux in the ripple bottom(top) case, because the center for the drift orbits is located between both focal points on the mid-plane.

Since the single-pass absorption in the case of ripple bottom resonance with O-mode injection is much weaker than that with X-mode injection, the most ECH powers are absorbed with X-mode after being partially transformed by the wall reflections in the case of the O-mode injection. Here, the optical depth τ_{opt} with X- and O- mode

estimated from the Bornatici's formula[27] are about 0.5 and 1×10^{-4} at $\rho = 0.5$ for target plasma, respectively. The ECH power absorption is less localized for the case of O-mode injection than that of X-mode injection. Therefore, the electrons interact more strongly with the wave at the ripple bottom resonance in the X-mode injection. The difference of the density decay between O- and X-mode injections is another support for the model that the enhancement of the particle flux with ECH is triggered by perpendicular acceleration of electrons.

The power absorption of even the X-mode ECH occurs at the resonance not only near the mid-plane but also in different region due to the multiple reflection at the vessel wall because of the poor single-pass absorption. Figure 6 also show the local resonance area normalized by the total resonance area $s(\rho)/S$[28] in the ripple bottom case. Here, the total resonance area S is defined as $\int_0^1 s(\rho)\mathrm{d}\rho$. The resonance area is not localized at $\rho = 0.5$(which is the focal point) but expands in the region outside of $\rho > 0.2$. As shown in Fig.6, when the electric field does not become positive (in the plasma with P_{ECH}=85kW), the particle flux Γ_{ECH} is enhanced with ECH only in $\rho > 0.2$. In that case, the particle flux is enhanced at the place where the ECH power is deposited. However, the particle flux Γ_{ECH} is enhanced even in $\rho < 0.2$ when the larger positive electric field is observed in the outer region($\rho > 0.6$). This suggests that the positive electric field in the outer region affects the particle flux in $\rho < 0.2$.

B. Evaluation of Radial Electric Field

Figure 8 shows the radial electric field profiles observed and evaluated theoretically for the plasma with ECH at the ripple bottom resonance (with $P_{\rm ECH}$=140kW), where the following nonlinear diffusion equation for the electric field[29] is used for the theoretical evaluation.

$$\frac{2}{\rho^2 a^2}\frac{\mathrm{d}}{\mathrm{d}\rho}[\rho^2 \hat{\eta}\,(E_{\rm r}' - \frac{E_{\rm r}}{\rho})] - \frac{1}{a^2}\frac{\partial \hat{\eta}}{\partial E_{\rm r}}(E_{\rm r}' - \frac{E_{\rm r}}{\rho})^2 = e[\Gamma_{\rm i}^{\rm NC}(E_{\rm r}) - \Gamma_{\rm e}^{\rm NC}(E_{\rm r}) - \Gamma_{\rm ECH}], \quad (3)$$

where the prime denotes the derivative on ρ. We assume that ECH enhances only electron particle flux, not ion particle flux, and that the anomalous particle fluxes are ambipolar. The dependence of the enhanced particle flux on the electric field is not taken into consideration. Here, $\hat{\eta}$ is such the factor that $\hat{\eta}\ B^2$ corresponds to the viscosity coefficient. The factor $\hat{\eta}\ B^2$ can be represented by a coefficient of shear viscosity $\mu^{\rm eff}$, $\hat{\eta}\ B^2 = n_{\rm i} m_{\rm i} \mu^{\rm eff}$. In this analysis, the coefficient $\mu^{\rm eff}$ is given as a constant parameter. Disagreement of the electric field profile between the observation and the calculation neglecting the viscosity term (at $\mu^{\rm eff}$=0 $\mathrm{m^2 s^{-1}}$) is clear. The calculated electric field is more positive at the plasma edge(ρ >0.8), and is more negative at the core region than the observed electric field. The scattering of the calculation comes from the error in the estimation of the enhanced particle flux $\Gamma_{\rm ECH}$ as shown in Fig.6. Since the calculation neglecting the viscosity term is based on the local flux balance on the each magnetic surface, the discontinuities in the electric field profile is caused. If the

change of the radial electric field to positive value occurs in the outer region, the electric field diffuses into the inner region under the influence of the perpendicular viscosity. Therefore, the theoretically evaluated electric field should become more smooth radial profile such as that of the observed electric field by taking the diffusion process of the electric field into consideration. As shown in Fig.8, the observed electric field profile is in well agreement with the theoretical prediction including the viscosity term, where $\mu_{\rm eff}$ =400m^{2}s^{-1} is used. The value of the coefficient $\mu_{\rm eff}$ is about one order larger than the measured ion thermal diffusivity. However, since we does not take into account the dependence of the factor $\hat{\eta}$ and $\Gamma_{\rm ECH}$ on the electric field, the further investigation is required for the quantitative comparison. The electric field that diffuses into the inner region may affect the particle flux in the region. The particle flux enhanced with ECH in the inner region where the resonance area does not exist($\rho < 0.2$) may be due to the influence of the diffused electric field on the particle flux. To discuss the formation of the positive electric field with ECH qualitatively, we restrict our results to the electric field at ρ=0.82.

Figure 9 shows a dependence of the observed electric field on the enhanced flux $\Gamma_{\rm ECH}$ at ρ=0.82 for the two resonance configurations. The change of the radial electric field from a negative to a positive value is observed at the larger enhanced flux($\sim 4 \times 10^{15}$cm^{-2}s^{-1}). Figure 10 shows the dependences of the ion and electron neoclas-

sical fluxes on the radial electric field for the plasma with ECH for the two resonance configurations at ρ=0.82. In the power scan experiment, since the obtained density and temperature profiles are not so different, the neoclassical fluxes estimated from the profiles change little. The ion neoclassical flux strongly depends on the radial electric field E_r and has a peak at $E_r \simeq 0$ in the ripple bottom case. The electron neoclassical flux has a weak dependence on the radial electric field in both two configurations. Since the temperature, especially of ion, in the ripple bottom case is observed to be higher than that in the ripple top case, as shown in Fig.3, due to the improvement of the confinement by the strong magnetic field, there is much difference between the neoclassical fluxes estimated from the density and temperature profiles in both configurations. However, the difference of the observed electric fields between two cases does not come from the change of the neoclassical fluxes or the obtained density and temperature profiles. In the ripple bottom case, the observed large positive electric field can not be explained by taking only the neoclassical fluxes into consideration as shown in Fig.10. The any additional electron loss is required to explain the positive electric field observed in the case of superposition of ECH on the NB heated plasmas. It is confirmed that the formation of the positive radial electric field can be realized using the enhanced particle flux which depends on the resonance positions and ECH power. The control of the electric field due to the injection modes is also found to be

effective.

V. CONCLUSION

It has been experimentally indicated that the radial electric field is controlled to positive value through the enhancement of the particle flux caused by ECH in CHS. The change of the electric field comes from the particle flux triggered by the production of the electrons accelerated perpendicularly to the magnetic field by ECH.

ACKNOWLEDGMENTS

One of the authors(H.I) wishes to express their thank Drs. M. Fujiwara and T. Watari for their encouragements and discussions. The authors would like to thank members of the torus experimental group for fruitful discussions and also to the technical staff for the operating ECH and NB systems. This work is partially supported by the Grant-in-Aid from a Ministry of Education, Science and Culture.

[1]H. E. Mynick and W. N. G. Hitchon, Nucl. Fusion **23**, 1053 (1983).

[2]L. M. Kovrizhnykh, Nucl. Fusion **24**, 435 (1984).

[3]D. E. Hastings, W. A. Houlberg and K. C. Shaing, Nucl. Fusion **25**, 445 (1985).

[4]K. Uo, A. Iiyoshi, T. Obiki, O. Motojima, S. Morimoto, A. Sasaki, K. Kondo, M. Sato, T. Mutoh, H. Zushi, H. Kaneko, S. Besshou, F. Sano, T. Mizuuchi, S. Sudo, K. Hanatani, M. Nakasuga, I. Ohtake, M. Iima, Y. Nakashima and N. Nishino, in *Plasma Physics and Controlled Nuclear Fusion Research, 1982*, Baltimore(International Atomic Energy Agency, Vienna, 1983) Vol.II p.209.

[5]K. Kondo, H. Zushi, S. Nishimura, H. Kaneko, M. Sato, S. Sudo, F. Sano, T. Mutoh, O. Motojima, T. Obiki, A. Iiyoshi and K. Uo, Rev. Sci. Instrum. **59**, 1533 (1988).

[6]G. Grieger, H. Renner and H. Wobig, Nucl. Fusion **25**, 1231 (1985).

[7]H. Wobig, H. Maassberg, H. Renner, The WVII-A Team, the ECRH Group and the NI Group, in *Plasma Physics and Controlled Nuclear Fusion Research, 1986*, Kyoto(International Atomic Energy Agency, Vienna, 1987) Vol.II p.369.

[8]J. F. Lyon, B. A. Carreras, K. K. Chipley, M. J. Cole, J. H. Harris, T. C. Jernigan, R. J. Johnson, V. E. Lynch, B. E. Nelson, J. A. Rome, J. Sheffield and P. B. Thompson, Fusion Technol. **10**, 179 (1986).

[9]S. C. Aceto, J. G. Schwelberger, K. A. Connor, J. J. Zielinski, J. C. Glowienka, R. C. Isler, M. Murakami, J. D. Bell and T. Uckan, in *Proceedings of 19th EPS Conf. on*

Controlled Fusion and Plasma Physics, Innsbruck, 1992 (European Physical Society, Petit-Lancy, 1992), Vol.16C part.I p.529.

[10]K. Matsuoka, S. Kubo, M. Hosokawa, Y. Takita, S. Okamura, N. Noda, H. Yamada, H. Iguchi, K. Masai, S. Morita, K. Ida, H. Idei, C. Takahashi, K. Nishimura, T. Shoji, H. Sanuki, M. Fujiwara, Y. Abe, T. Amano, A. Ando, T. Aoki, D.-G.Bi, J. Fujita, S. Hidekuma, T. Kamimura, O. Kaneko, T. Kawamoto, A. Mohri, A. Nishizawa, S. Tanahashi, J. Todoroki, K. Tsuzuki and K. Yamazaki, in *Plasma Physics and Controlled Nuclear Fusion Research, 1988*, Nice(International Atomic Energy Agency, Vienna, 1989) Vol.II p.411.

[11]K. Ida, H. Yamada, H. Iguchi, S. Hidekuma, H. Sanuki, K. Yamazaki and the CHS Group, Phys. Fluids B**3**, 515 (1991); B**4**, 1360 (1992).

[12]H. Idei, K. Ida, H. Sanuki, H. Yamada, H. Iguchi, S. Kubo, R. Akiyama, H. Arimoto, M. Fujiwara, M. Hosokawa, K. Matsuoka, S. Morita, K. Nishimura, K. Ohkubo, S. Okamura, S. Sakakibara, C. Takahashi, Y. Takita, K. Tsumori and I. Yamada, Phys. Rev. Lett. **71**, 2220(1993).

[13]H. Hsuan, K. Bol, N. Bowen, D. Boyd, A. Cavallo, A. Dimits, J. Doane, G. Elder, M. Goldman, B. Grek, C. Hoot, D. Jonson, A. Kritz, B. LeBlanc, P. Manintveld, R. Polman, S. Sesnic, H. Takahashi and F. Terry, in *Proceedings of 4th Int. Symp. on Heating in Toroidal Plasmas*, Rome, 1984 (International School of Plasma Physics,

Varenna, 1984), Vol.II p.809.

[14]F. Sardei, H. Ringler, A. Dodhy, G. Kühner, WVII-AS Group and ECRH Group, in *Proceedings of 17th EPS Conf. on Controlled Fusion and Plasma Heating*, Amsterdam, 1990 (European Physical Society, Petit-Lancy, 1990), Vol.14B part II p.471.

[15]H. Zushi, M. Sato, O. Motojima, S. Sudo, T. Mutoh, K. Kondo, H. Kaneko, T. Mizuuchi, H. Okada, Y. Takeiri, F. Sano, A. Iiyoshi and K. Uo, Nucl. Fusion **28**, 1801 (1988).

[16]H. Idei, S. Kubo, H. Sanuki, H. Iguchi, K. Ida, S. Morita, R. Akiyama, H. Arimoto, K. Matsuoka, K. Nishimura, K. Ohkubo, S. Okamura, C. Takahashi, Y. Takita, K. Toi, K. Tsumori, H. Yamada and I. Yamada, "Experimental Study on Density Pump-Out due to Electron Cyclotron Heating in the CHS Heliotron/Torsatron," accepted for publication in Fusion Eng. Design (Proc. of 5th Int. Toki Conf.).

[17]D. Meade, W. Arunasalam, C. Barnes, K. Bol, S. Cohen, H. Dalhed, C. Daughney, S. Davis, J. DeLucia, D. Dimock, F. Dylla, P. Efthimion, R. Fonck, B. Grek, R. Hawryluk, E. Hinnov, H. Hsuan, M. Irie, R. Jacobsen, D. Johnson, L. Johnson, H. Maeda, D. Mansfield, G. McCracken, D. Mueller, M. Okabayashi, O. Okada, K. Owens, S. Picraux, S. Rossnagel, N. Sauthoff, G. Schmidt, J. Schmidt, E. Silver, J. Sinnis, P. Staib, J. Strachan, S. Suckewer, F. Tenney and W. Wampler, in *Proceedings of 9th EPS Conf. on Controlled Fusion and Plasma Physics*, Oxford, 1979 (European Physical Society,

Petit-Lancy, 1979), p.91.

[18]S. Kubo, H. Idei, M. Hosokawa, Y. Takita, H. Iguchi, I. Yamada, H. Arimoto, M. Ueda, K. Ida, K. Matsuoka, S. Morita, K. Nishimura, S. Okamura, C. Takahashi, H. Yamada, M. Fujiwara, N. Noda, A. Sagara, H. Sanuki, J. Todoroki and K. Toi, in *Proceedings of 19th EPS Conf. on Controlled Fusion and Plasma Physics*, Innsbruck, 1992 (European Physical Society, Petit-Lancy, 1992), Vol.16C part.I p.513.

[19]O. Kaneko, S. Kubo, K. Nishimura, T. Shoji, M. Hosokawa, K. Ida, H. Idei, H. Iguchi, K. Matsuoka, S. Morita, N. Noda, S. Okamura, T. Ozaki, A. Sagara, H. Sanuki, C. Takahashi, Y. Takeiri, Y. Takita, K. Tsuzuki, H. Yamada, T. Amano, A. Ando, M. Fujiwara, K. Hanatani, A. Karita, T. Kohmoto, A. Komori, K. Masai, T. Morisaki, O. Motojima, N. Nakajima, Y. Oka, M. Okamoto, S. Sobhanian and J. Todoroki, in *Plasma Physics and Controlled Nuclear Fusion Research, 1990*, Washington(International Atomic Energy Agency, Vienna, 1991) Vol.II p.473.

[20]K. Ida and S. Hidekuma, Rev. Sci. Instrum. **60**, 876 (1989).

[21]K. Ida, H. Yamada, H. Iguchi, K. Itoh and CHS Group, Phys. Rev. Lett. **67**, 58 (1991).

[22]S. P. Hirshman, W. I. van Rij and P. Merkel, Comput. Phys. Commun. **43**, 143 (1986).

[23]H. Yamada, K. Ida, H. Iguchi, S. Morita, O. Kaneko, H. Arimoto, M. Hosokawa, H.

Idei, S. Kubo, K. Matsuoka, K. Nishimura, S. Okamura, Y. Takeiri, Y. Takita, C. Takahashi, K. Hanatani, H. C. Howe, S. P. Hirshman and D. K. Lee, Nucl. Fusion **32**, 25 (1992).

[24]K. Itoh, S.-I. Itoh, and A. Fukuyama, J. Phys. Soc. Japan **58**, 482 (1989).

[25]H. Sanuki, J. Todoroki and T. Kamimura, Phys. Fluids B**2**, 2155 (1990).

[26]M. D. Carter, J. D. Callen, D. B. Batchelor and R. C. Goldfinger, Phys. Fluids **29**, 100 (1986).

[27]M. Bornatici, Plasma Physics **24**, 629 (1982).

[28]H. Idei, S. Kubo, M. Hosokawa, H. Iguchi, K. Ohkubo, T. Sato and CHS group, Jpn. J. Appl. Phys. **33** Part 1, 1543 (1994).

[29]H. Maassberg, R. Burhenn, U. Gasparino, G. Kühner, H. Ringler and K. S. Dyabilin, Phys. Fluids B**5**, 3627 (1993).

Figure Captions

FIG.1 : Schematic drawing of resonance structure at high field side(ripple top) and low field side(ripple bottom) resonance.

FIG.2 : Radial profiles of electron density for the reference plasma, the target plasmas and those with ECH at (a)ripple top and (b)ripple bottom resonances.

FIG.3 : Radial profiles of (a)electron temperature, (b)ion temperature, (c)poloidal rotation velocity and (d)radial electric field for the reference plasma and those with ECH at the ripple top and bottom resonances.

FIG.4 : Radial profiles of radial electric field for the reference plasma and those with the injection power P_{ECH}=85 and 140kW at ripple bottom resonance.

FIG.5 : (a)Time evolutions of density decay $\Delta\bar{n}_{\mathrm{e}}$ and (b)radial profiles of poloidal rotation velocity $v_{\theta}(\rho)$ for the plasmas with ECH of O- and X- mode injections, respectively. Here, $\Delta\bar{n}_{\mathrm{e}}$ shows the difference of the line-averaged density between the NB heated target plasma and that with ECH.

FIG.6 : Radial profiles of enhanced fluxes Γ_{ECH} for the plasmas with the injection power P_{ECH}=85 and 140kW at the ripple bottom resonance, and a neoclassical flux

Γ^{NC} for the target plasma. Radial profile of normalized resonance area in the ripple bottom case is also shown.

FIG.7 : Ratios ν_{eff}/ν_{rf} and τ_{rf}/τ_{pas}, and increase of the energy accelerated by the nonlinear wave-particle interaction versus initial electron energy. Here, ν_{eff} is effective randomization frequency, and $\tau_{rf}(\equiv 1/\nu_{rf})$ and τ_{pas} are the excursion time due to the nonlinear interaction and passing time of electrons through the resonance area, respectively.

FIG.8 : Radial electric field profiles for the plasma with ECH at the ripple bottom resonance(with P_{ECH}=140kW). Closed circles show the observed electric fields. Hatched areas show the electric fields calculated from the diffusion equation of the electric field neglecting the viscosity term and taking into account the term, respectively. The hatched areas come from the error in estimation of the enhanced particle flux Γ_{ECH} as shown in Fig.6.

FIG.9 : Observed radial electric fields E_r versus enhanced fluxes Γ_{ECH} at ρ=0.82 for the plasmas with ECH at ripple top and bottom resonances.

FIG.10 : Dependences of ion and electron neoclassical fluxes, Γ_i^{NC} and Γ_e^{NC}, on radial electric field E_r for the plasma with ECH at $\rho = 0.82$ in cases of ripple top

and bottom resonances. Closed circles show the points which satisfy the ambipolarity equation, $\Gamma_e^{NC} = \Gamma_i^{NC}$.

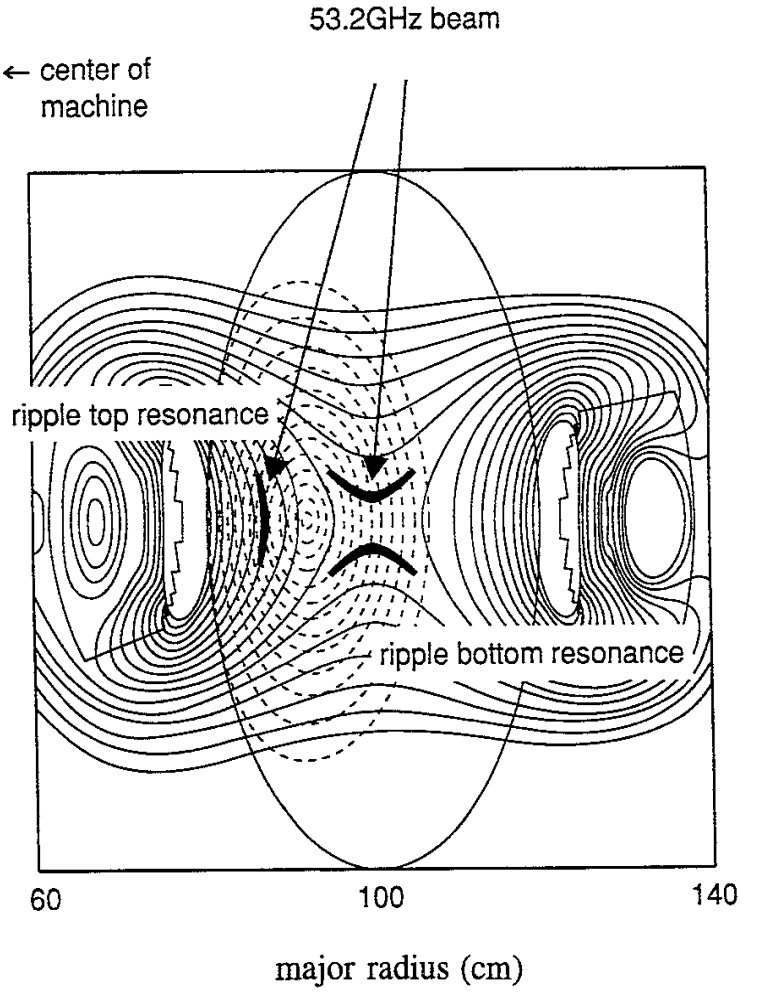
53.2GHz beam
← center of machine
ripple top resonance
ripple bottom resonance
60
100
140
major radius (cm)

FIG.1

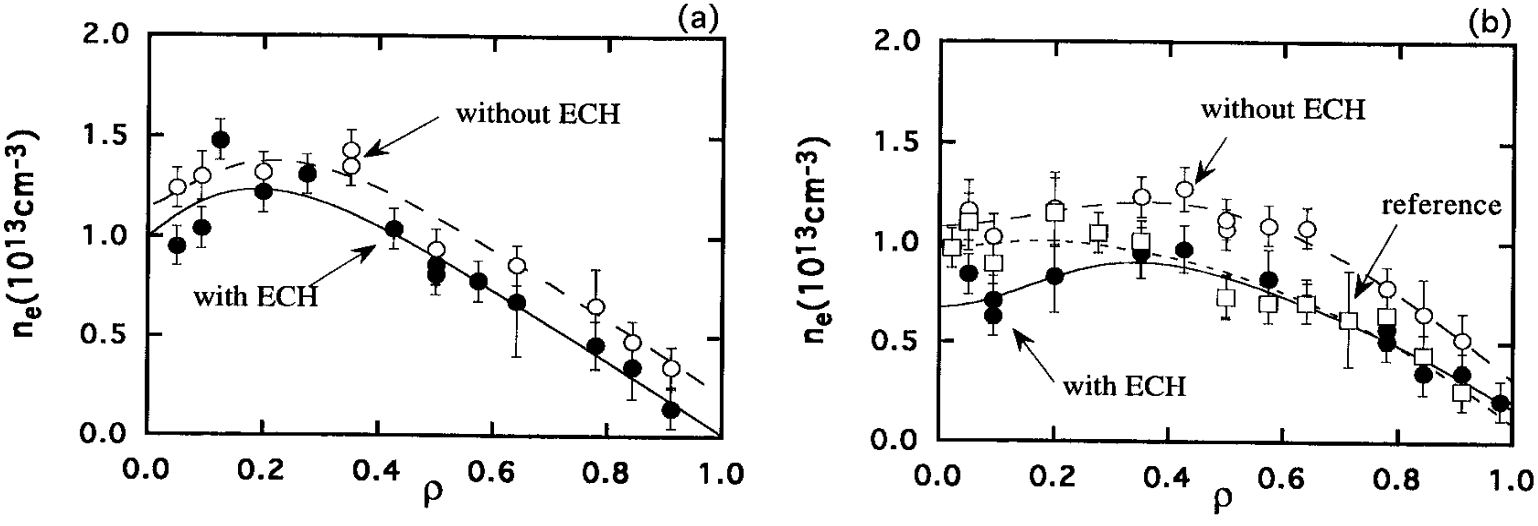
(a)
2.0
1.5
1.0
0.5
0.0
$n_e(10^{13}cm^{-3})$
without ECH
with ECH
0.0
0.2
0.4
0.6
0.8
1.0
ρ
(b)
2.0
1.5
1.0
0.5
0.0
$n_e(10^{13}cm^{-3})$
without ECH
reference
with ECH
0.0
0.2
0.4
0.6
0.8
1.0
ρ

FIG.2

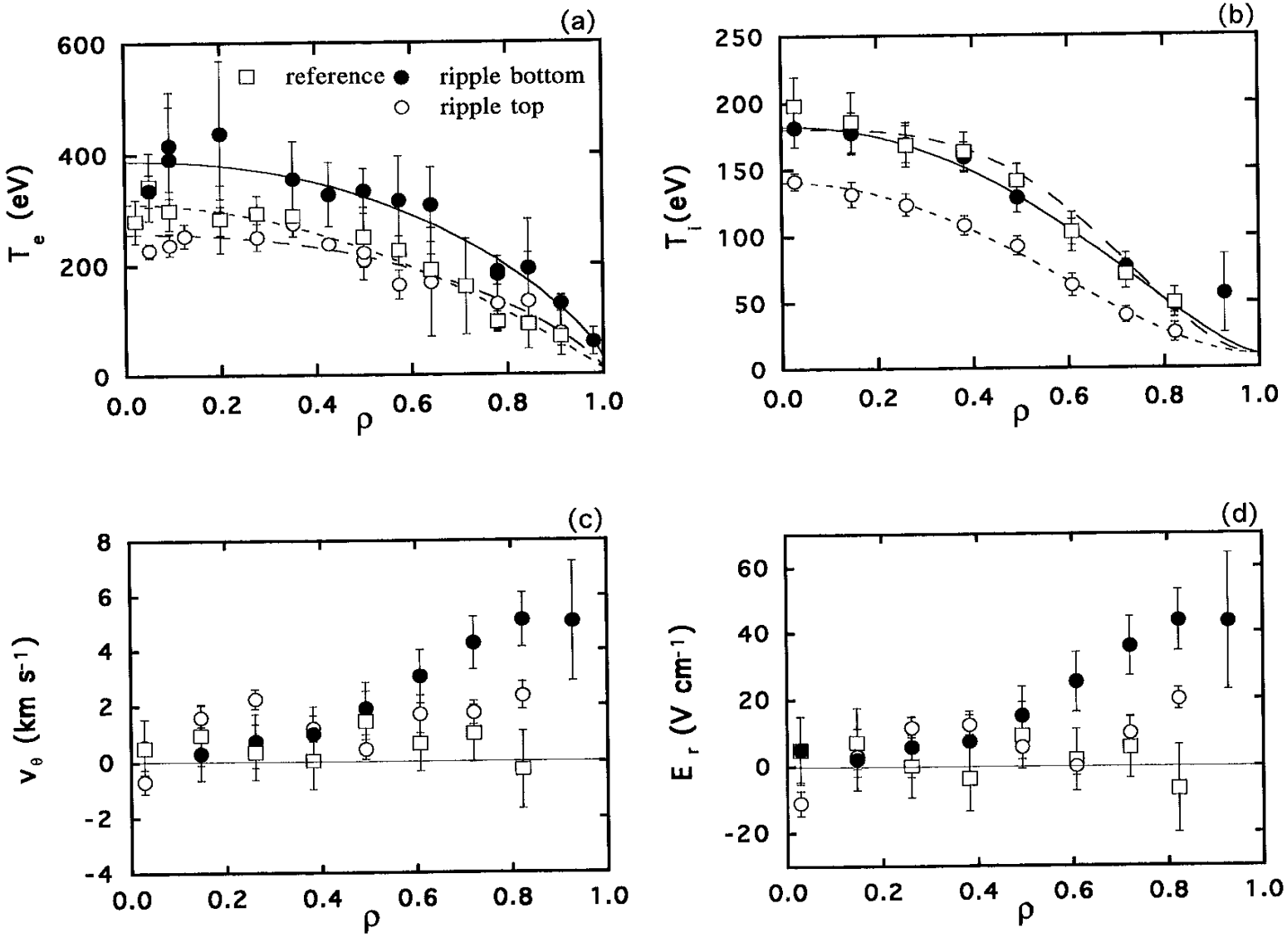
(a)
reference
ripple bottom
ripple top
T_e (eV)
600
400
200
0
0.0
0.2
0.4
0.6
0.8
1.0
ρ
(b)
T_i (eV)
250
200
150
100
50
0
0.0
0.2
0.4
0.6
0.8
1.0
ρ
(c)
v_θ (km s^{-1})
8
6
4
2
0
-2
-4
0.0
0.2
0.4
0.6
0.8
1.0
ρ
(d)
E_r (V cm^{-1})
60
40
20
0
-20
0.0
0.2
0.4
0.6
0.8
1.0
ρ

FIG.3

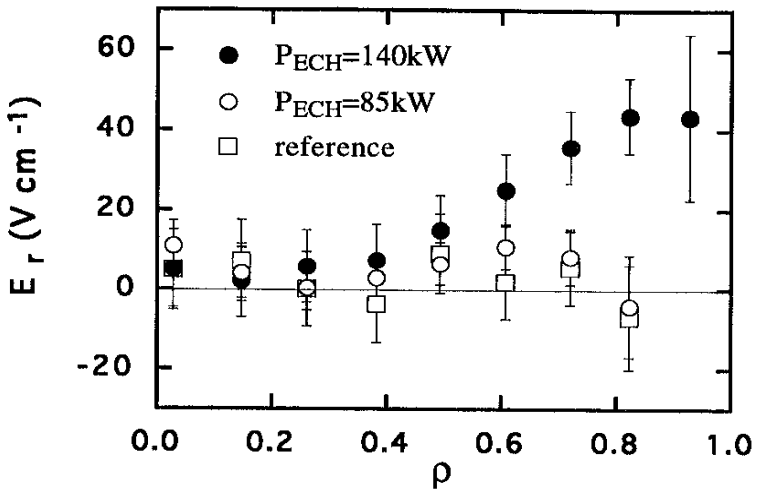
60
40
20
0
-20
0.0
0.2
0.4
0.6
0.8
1.0
ρ
E r (V cm -1)
P ECH=140kW
P ECH=85kW
reference

FIG.4

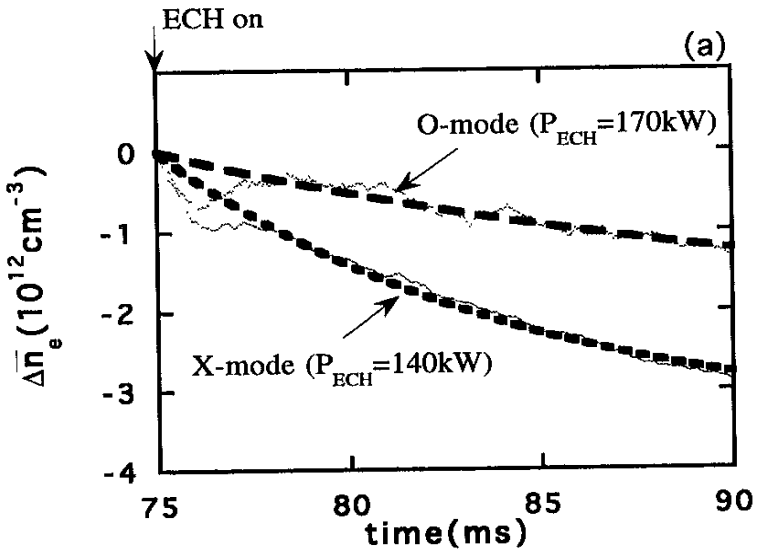
ECH on
(a)
O-mode (P_{ECH}=170kW)
X-mode (P_{ECH}=140kW)
$\Delta\bar{n}_e$ (10^{12}cm^{-3})
0
-1
-2
-3
-4
75
80
85
90
time(ms)

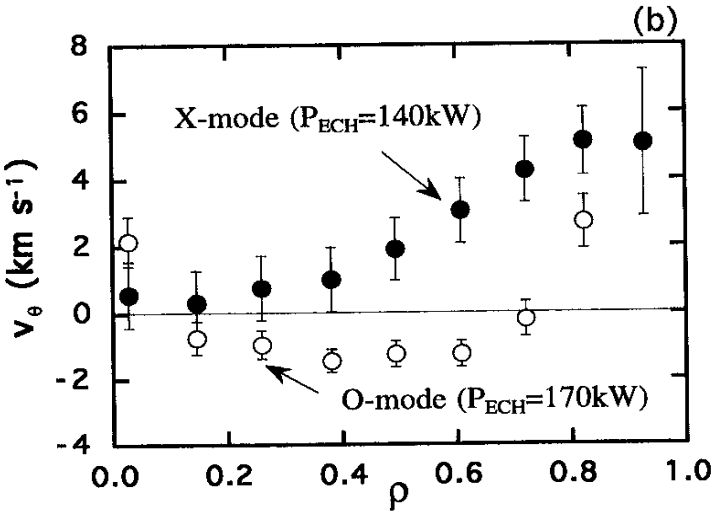
(b)
X-mode (P_{ECH}=140kW)
O-mode (P_{ECH}=170kW)
v_θ (km s^{-1})
8
6
4
2
0
-2
-4
0.0
0.2
0.4
0.6
0.8
1.0
ρ

FIG.5

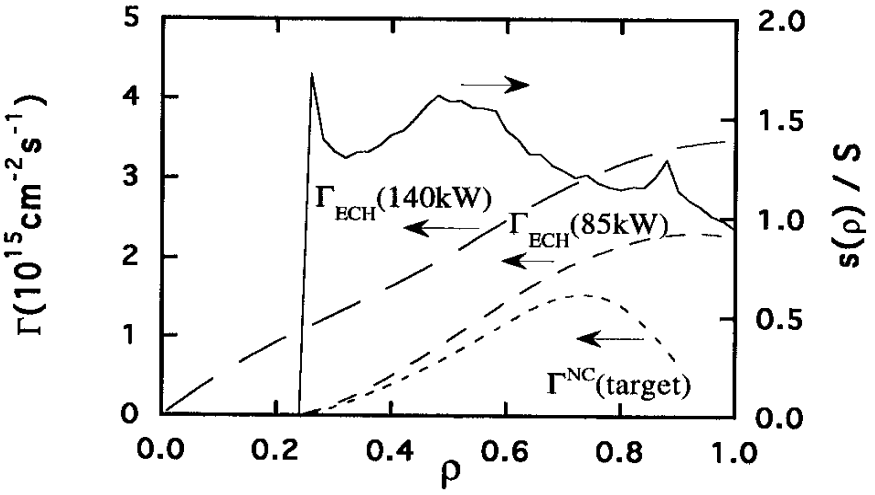
5
4
3
2
1
0
2.0
1.5
1.0
0.5
0.0
0.0
0.2
0.4
0.6
0.8
1.0
ρ
Γ(10^15 cm^-2 s^-1)
s(ρ) / S
Γ_ECH(140kW)
Γ_ECH(85kW)
Γ^NC(target)

FIG.6

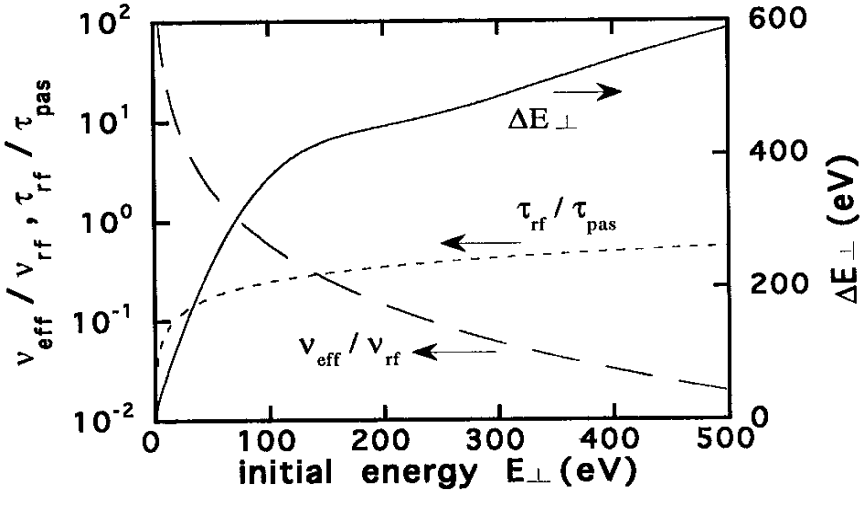
10^2
10^1
10^0
10^{-1}
10^{-2}
ν_{eff} / ν_{rf} , τ_{rf} / τ_{pas}
600
400
200
0
$\Delta E_\perp$ (eV)
$\Delta E_\perp$
τ_{rf} / τ_{pas}
ν_{eff} / ν_{rf}
0
100
200
300
400
500
initial energy $E_\perp$ (eV)

FIG.7

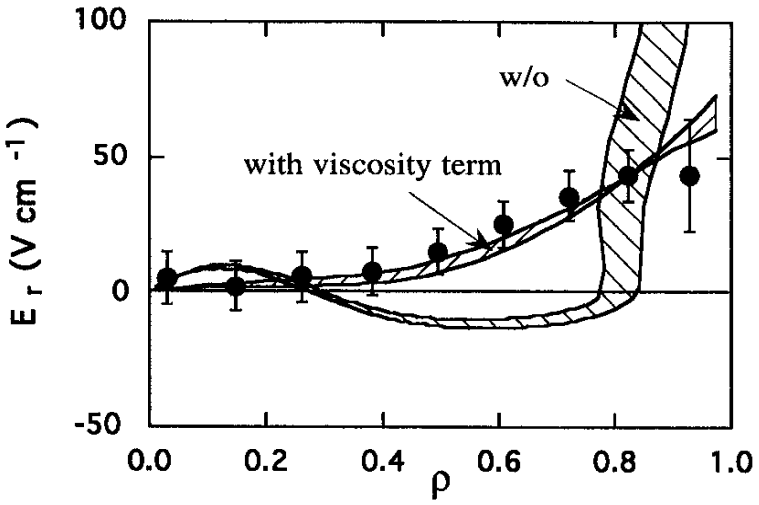

FIG.8

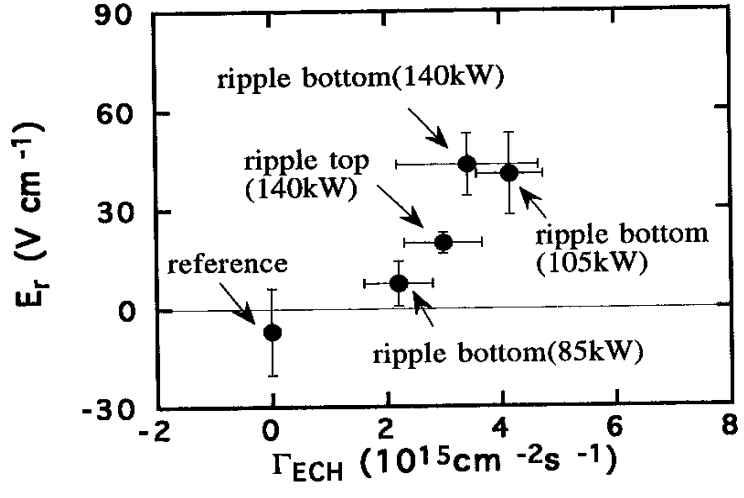
90
60
30
0
-30
-2
0
2
4
6
8
E_r (V cm $^{-1}$)
Γ_{ECH} (10^{15}cm $^{-2}$s $^{-1}$)
ripple bottom(140kW)
ripple top
(140kW)
ripple bottom
(105kW)
reference
ripple bottom(85kW)

FIG.9

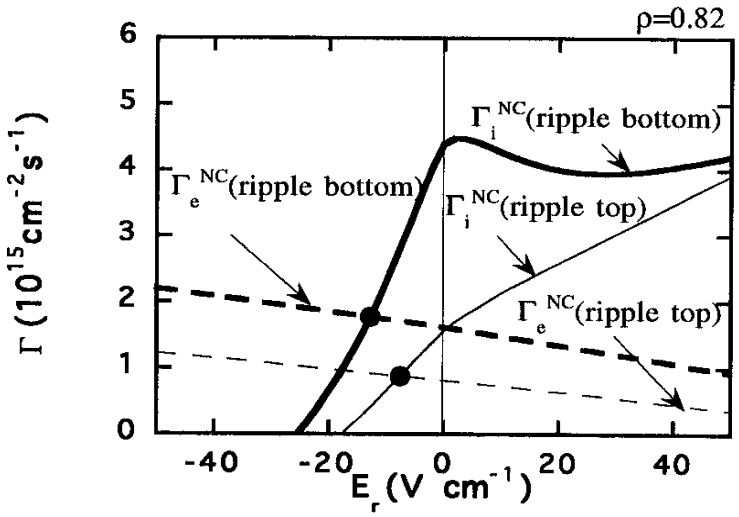
ρ=0.82
6
5
4
3
2
1
0
-40
-20
0
20
40
Γ (10^15 cm^-2 s^-1)
E_r (V cm^-1)
Γ_i^NC(ripple bottom)
Γ_e^NC(ripple bottom)
Γ_i^NC(ripple top)
Γ_e^NC(ripple top)

FIG.10

Recent Issues of NIFS Series

NIFS-247 T. Yamagishi,
Trapped Electron Instabilities due to Electron Temperature Gradient and Anomalous Transport; Oct. 1993

NIFS-248 Y. Kondoh,
Attractors of Dissipative Structure in Three Disspative Fluids; Oct. 1993

NIFS-249 S. Murakami, M. Okamoto, N. Nakajima, M. Ohnishi, H. Okada,
Monte Carlo Simulation Study of the ICRF Minority Heating in the Large Helical Device; Oct. 1993

NIFS-250 A. Iiyoshi, H. Momota, O. Motojima, M. Okamoto, S. Sudo, Y. Tomita, S. Yamaguchi, M. Ohnishi, M. Onozuka, C. Uenosono,
Innovative Energy Production in Fusion Reactors; Oct. 1993

NIFS-251 H. Momota, O. Motojima, M. Okamoto, S. Sudo, Y. Tomita, S. Yamaguchi, A. Iiyoshi, M. Onozuka, M. Ohnishi, C. Uenosono,
Characteristics of D-^{3}He Fueled FRC Reactor: ARTEMIS-L,
Nov. 1993

NIFS-252 Y. Tomita, L.Y. Shu, H. Momota,
Direct Energy Conversion System for D-^{3}He Fusion, Nov. 1993

NIFS-253 S. Sudo, Y. Tomita, S. Yamaguchi, A. Iiyoshi, H. Momota, O. Motojima, M. Okamoto, M. Ohnishi, M. Onozuka, C. Uenosono,
Hydrogen Production in Fusion Reactors, Nov. 1993

NIFS-254 S. Yamaguchi, A. Iiyoshi, O. Motojima, M. Okamoto, S. Sudo, M. Ohnishi, M. Onozuka, C. Uenosono,
Direct Energy Conversion of Radiation Energy in Fusion Reactor,
Nov. 1993

NIFS-255 S. Sudo, M. Kanno, H. Kaneko, S. Saka, T. Shirai, T. Baba,
Proposed High Speed Pellet Injection System "HIPEL" for Large Helical Device
Nov. 1993

NIFS-256 S. Yamada, H. Chikaraishi, S. Tanahashi, T. Mito, K. Takahata, N. Yanagi, M. Sakamoto, A. Nishimura, O. Motojima, J. Yamamoto, Y. Yonenaga, R. Watanabe,
Improvement of a High Current DC Power Supply System for Testing the Large Scaled Superconducting Cables and Magnets; Nov. 1993

NIFS-257 S. Sasaki, Y. Uesugi, S. Takamura, H. Sanuki, K. Kadota,
Temporal Behavior of the Electron Density Profile During Limiter Biasing in the HYBTOK-II Tokamak; Nov. 1993

NIFS-258 K. Yamazaki, H. Kaneko, S. Yamaguchi, K.Y. Watanabe, Y.Taniguchi, O.Motojima, LHD Group,
Design of Central Control System for Large Helical Device (LHD); Nov. 1993

NIFS-259 S. Yamada, T. Mito, A. Nishimura, K. Takahata, S. Satoh, J. Yamamoto, H. Yamamura, K. Masuda, S. Kashihara, K. Fukusada, E. Tada,
Reduction of Hydrocarbon Impurities in 200L/H Helium Liquefier-Refrigerator System; Nov. 1993

NIFS-260 B.V.Kuteev,
Pellet Ablation in Large Helical Device; Nov. 1993

NIFS-261 K. Yamazaki,
Proposal of "MODULAR HELIOTRON': Advanced Modular Helical System Compatible with Closed Helical Divertor; Nov. 1993

NIFS-262 V.D.Pustovitov,
Some Theoretical Problems of Magnetic Diagnostics in Tokamaks and Stellarators; Dec. 1993

NIFS-263 A. Fujisawa, H. Iguchi, Y. Hamada
A Study of Non-Ideal Focus Properties of 30° Parallel Plate Energy Analyzers; Dec. 1993

NIFS-264 K. Masai,
Nonequilibria in Thermal Emission from Supernova Remnants; Dec. 1993

NIFS-265 K. Masai, K. Nomoto,
X-Ray Enhancement of SN 1987A Due to Interaction with its Ring-like Nebula; Dec. 1993

NIFS-266 J. Uramoto
A Research of Possibility for Negative Muon Production by a Low Energy Electron Beam Accompanying Ion Beam; Dec. 1993

NIFS-267 H. Iguchi, K. Ida, H. Yamada, K. Itoh, S.-I. Itoh, K. Matsuoka, S. Okamura, H. Sanuki, I. Yamada, H. Takenaga, K. Uchino, K. Muraoka,
The Effect of Magnetic Field Configuration on Particle Pinch Velocity in Compact Helical System (CHS); Jan. 1994

NIFS-268 T. Shikama, C. Namba, M. Kosuda, Y. Maeda,
Development of High Time-Resolution Laser Flash Equipment for Thermal Diffusivity Measurements Usting Miniature-Size Specimens; Jan. 1994

NIFS-269 T. Hayashi, T. Sato, P. Merkel, J. Nührenberg, U. Schwenn,

Formation and 'Self-Healing' of Magnetic Islands in Finite-β Helias Equilibria; Jan. 1994

NIFS-270 S. Murakami, M. Okamoto, N. Nakajima, T. Mutoh,
Efficiencies of the ICRF Minority Heating in the CHS and LHD Plasmas; Jan. 1994

NIFS-271 Y. Nejoh, H. Sanuki,
Large Amplitude Langmuir and Ion-Acoustic Waves in a Relativistic Two-Fluid Plasma; Feb. 1994

NIFS-272 A. Fujisawa, H. Iguchi, A. Taniike, M. Sasao, Y. Hamada,
A 6MeV Heavy Ion Beam Probe for the Large Helical Device;
Feb. 1994

NIFS-273 Y. Hamada, A. Nishizawa, Y. Kawasumi, K. Narihara, K. Sato, T. Seki, K. Toi, H. Iguchi, A. Fujisawa, K. Adachi, A. Ejiri, S. Hidekuma, S. Hirokura, K. Ida, J. Koong, K. Kawahata, M. Kojima, R. Kumazawa, H. Kuramoto, R. Liang, H. Sakakita, M. Sasao, K. N. Sato, T. Tsuzuki, J. Xu, I. Yamada, T. Watari, I. Negi,
Measurement of Profiles of the Space Potential in JIPP T-IIU Tokamak Plasmas by Slow Poloidal and Fast Toroidal Sweeps of a Heavy Ion Beam; Feb. 1994

NIFS-274 M. Tanaka,
A Mechanism of Collisionless Magnetic Reconnection; Mar. 1994

NIFS-275 A. Fukuyama, K. Itoh, S.-I. Itoh, M. Yagi and M. Azumi,
Isotope Effect on Confinement in DT Plasmas; Mar. 1994

NIFS-276 R.V. Reddy, K. Watanabe, T. Sato and T.H. Watanabe,
Impulsive Alfven Coupling between the Magnetosphere and Ionosphere; Apr.1994

NIFS-277 J. Uramoto,
A Possibility of π^- Meson Production by a Low Energy Electron Bunch and Positive Ion Bunch; Apr. 1994

NIFS-278 K. Itoh, S.-I. Itoh, A. Fukuyama, M. Yagi and M. Azumi,
Self-sustained Turbulence and L-mode Confinement in Toroidal Plasmas II; Apr. 1994

NIFS-279 K. Yamazaki and K.Y.Watanabe,
New Modular Heliotron System Compatible with Closed Helical Divertor and Good Plasma Confinement; Apr. 1994

NIFS-280 S. Okamura, K. Matsuoka, K. Nishimura, K. Tsumori, R. Akiyama, S. Sakakibara, H. Yamada, S. Morita, T. Morisaki,. N. Nakajima,

K. Tanaka, J. Xu, K. Ida, H. Iguchi, A. Lazaros, T. Ozaki, H. Arimoto, A. Ejiri, M. Fujiwara, H. Idei. O. Kaneko, K. Kawahata, T. Kawamoto, A. Komori, S. Kubo, O. Motojima, V.D. Pustovitov, C. Takahashi, K. Toi and I. Yamada,
High-Beta Discharges with Neutral Beam Injection in CHS, Apr; 1994

NIFS-281 K. Kamada, H. Kinoshita and H. Takahashi,
Anomalous Heat Evolution of Deuteron Implanted Al on Electron Bombardment ; May 1994

NIFS-282 H. Takamaru, T. Sato, K. Watanabe and R. Horiuchi,
Super Ion Acoustic Double Layer; May 1994

NIFS-283 O.Mitarai and S. Sudo
Ignition Characteristics in D-T Helical Reactors; June 1994

NIFS-284 R. Horiuchi and T. Sato,
Particle Simulation Study of Driven Magnetic Reconnection in a Collisionless Plasma; June 1994

NIFS-285 K.Y. Watanabe, N. Nakajima, M. Okamoto, K. Yamazaki, Y. Nakamura, M. Wakatani,
Effect of Collisionality and Radial Electric Field on Bootstrap Current in LHD (Large Helical Device); June 1994

NIFS-286 H. Sanuki, K. Itoh, J. Todoroki, K. Ida, H. Idei, H. Iguchi and H. Yamada,
Theoretical and Experimental Studies on Electric Field and Confinement in Helical Systems; June 1994

NIFS-287 K. Itoh and S-I. Itoh,
Influence of the Wall Material on the H-mode Performance; June 1994

NIFS-288 K. Itoh, A. Fukuyama, S.-I. Itoh, M. Yagi and M. Azumi
Self-Sustained Magnetic Braiding in Toroidal Plasmas July 1994

NIFS-289 Y. Nejoh,
Relativistic Effects on Large Amplitude Nonlinear Langmuir Waves in a Two-Fluid Plasma; July 1994

NIFS-290 N. Ohyabu, A. Komori, K. Akaishi, N. Inoue, Y. Kubota, A.I. Livshit, N. Noda, A. Sagara, H. Suzuki, T. Watanabe, O. Motojima, M. Fujiwara, A. Iiyoshi,
Innovative Divertor Concepts for LHD; July 1994